Supporting Information

Unraveling the reversible formation of defective Ce^{3+} sites in the UiO-66(Ce) material: a multi-technique study

Sergio Rojas-Buzo, Davide Salusso, Francesca Bonino, Maria Cristina Paganini and Silvia Bordiga**

X-ray Diffraction

The resultant solids show the characteristic PXRD pattern of the UiO-66 material. The shift towards higher 2θ when the amount of Zr is increased is consistent with the shorter ionic radius of eight-fold coordinated Zr^{4+} in comparison with Ce^{4+} (see Figure S1).[1]

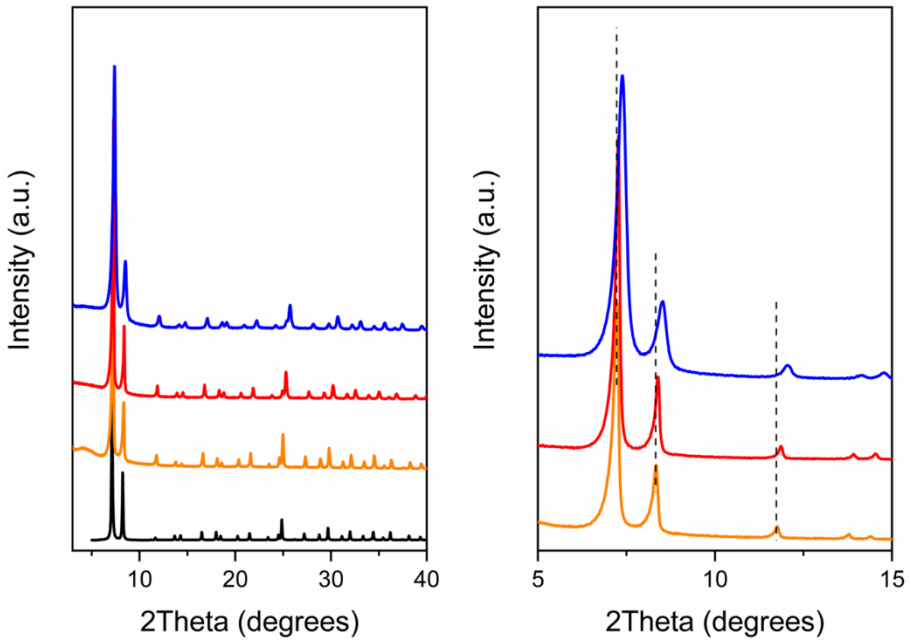

Figure S1. PXRD patterns of the simulated UiO-66(Ce) (black line), as-synthesized UiO-66(Ce) (orange line), UiO-66($Ce_{0.5}Zr_{0.5}$) (red line) and UiO-66($Ce_{0.05}Zr_{0.95}$) (blue line).

Thermogravimetric analysis

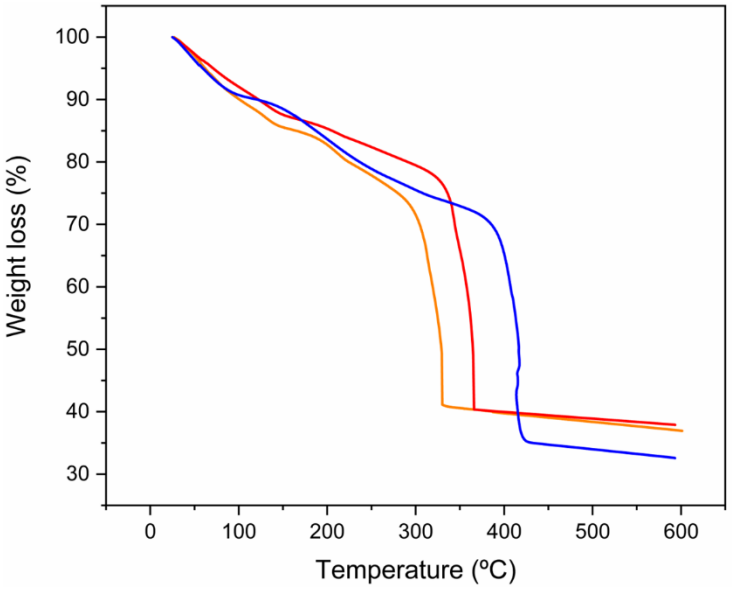

Figure S2. Thermogravimetric analysis of the UiO-66(Ce) (orange line), UiO-66($Ce_{0.5}Zr_{0.5}$) (red line) and UiO-66($Ce_{0.05}Zr_{0.95}$) (blue line). The increase in the amount of Zr is associated with sample thermal stability increment.[2]

N_2 adsorption

In all the cases, type I isotherms were observed, which are characteristic of microporous materials (see Figure S3). The calculated BET area for the materials synthesized in this work increase with the proportion of Zr as has been yet reported in the literature (~1311 and ~1444 m^2/g for the UiO-66($Ce_{0.5}Zr_{0.5}$) and UiO-66($Ce_{0.05}Zr_{0.95}$), respectively).[3]

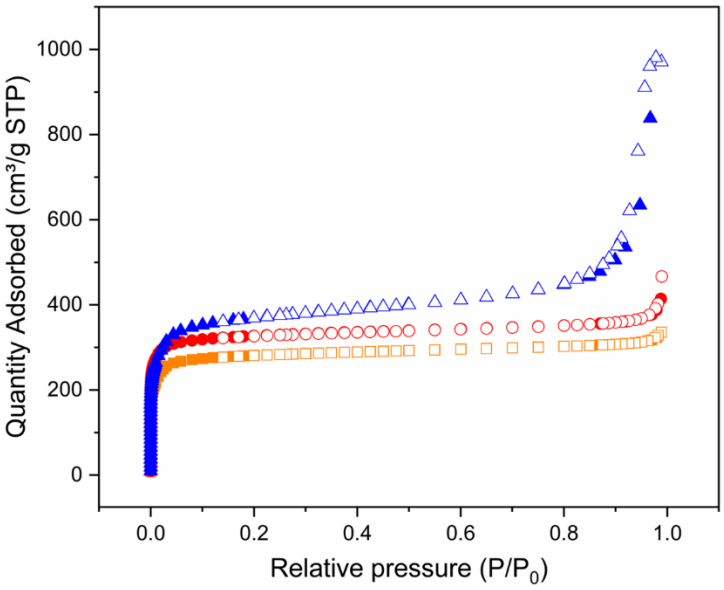

Figure S3. N_2 adsorption-desorption isotherms of UiO-66(Ce) (orange squares), UiO-66($Ce_{0.5}Zr_{0.5}$) (red circles) and UiO-66($Ce_{0.05}Zr_{0.95}$) (blue triangles).

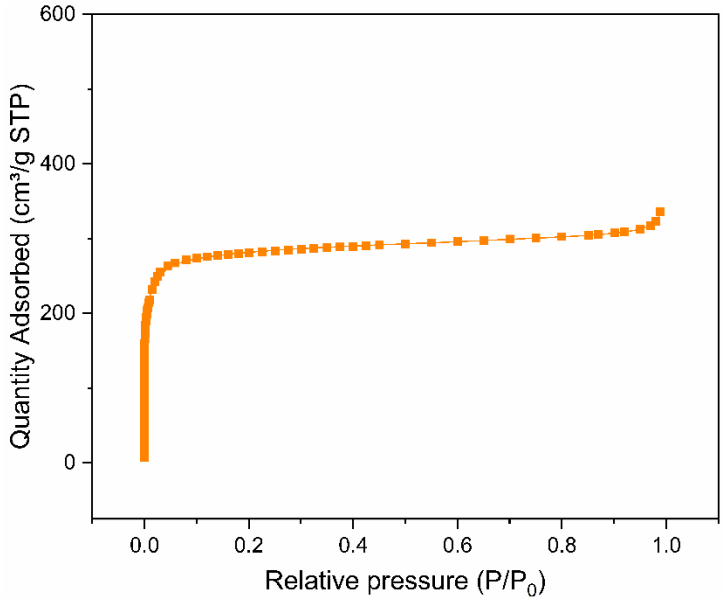

Figure S4. N_2 adsorption isotherm of UiO-66(Ce) (orange squares) together with the fitting obtained by the N_2-Cylindrical Pores-Oxide Surface DFT model (orange line).

Tauc plots

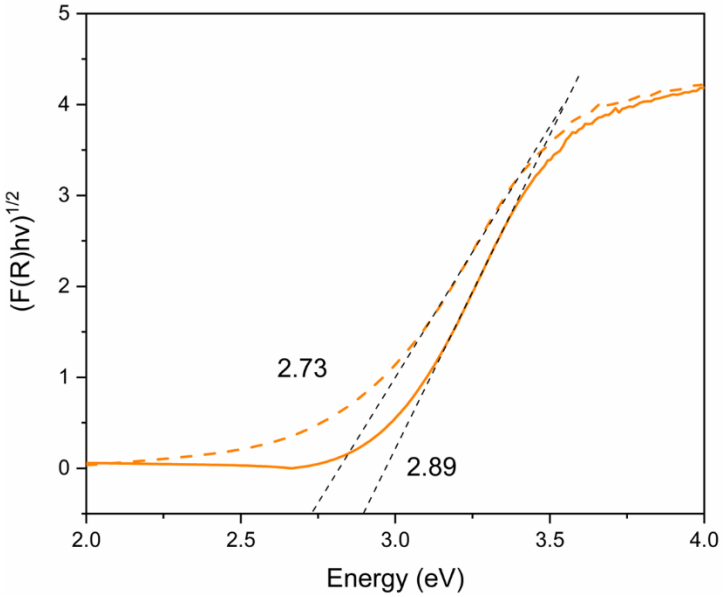

Figure S5. Tauc plots for the UiO-66(Ce). As-synthesized (solid line) and activated at 110ºC (dash line).

XPS

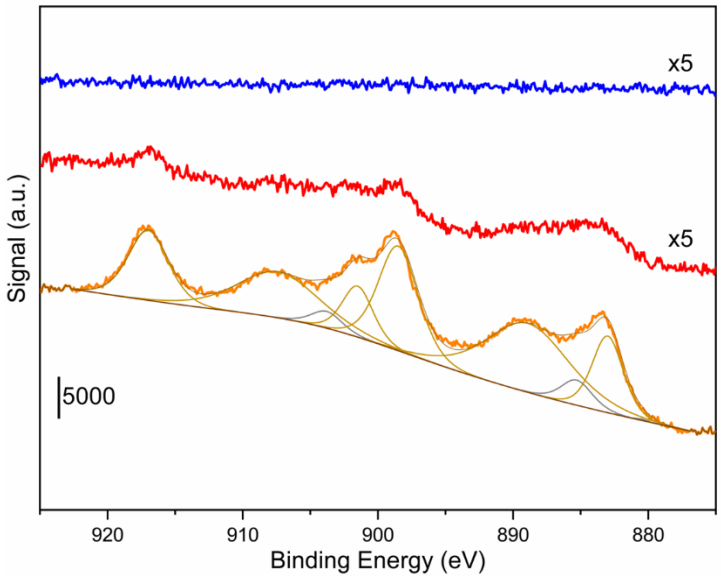

Figure S6. Ce(3d) XPS spectra for UiO-66(Ce) (orange line), UiO-66($Ce_{0.5}Zr_{0.5}$) (red line) and UiO-66($Ce_{0.05}Zr_{0.95}$) (blue line). Ce^{3+} and Ce^{4+} components are shown with yellow and black lines, respectively.

NEXAFS

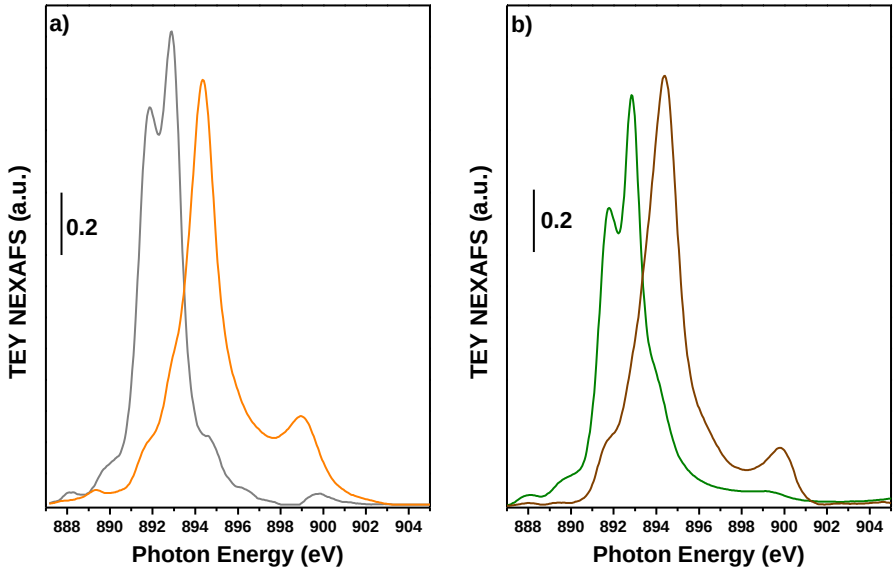

Figure S7. TEY NEXAFS spectra a) pure Ce^{4+} (orange line) and Ce^{3+} (grey line) components extracted from MCR-ALS procedure and b) of reference CeO_2 (brown) and CeF_3 (green line).

UV-Vis absorption

When the amount of Zr is increased in the Ce_xZr_{6-x} clusters (from x=6 to x=0.3), a blue shift in the UV adsorption profile is observed (see Figure S6). This could be ascribed to the fact that zirconia absorbs at lower wavelengths than ceria (around 275 and 400 nm, respectively).[4]

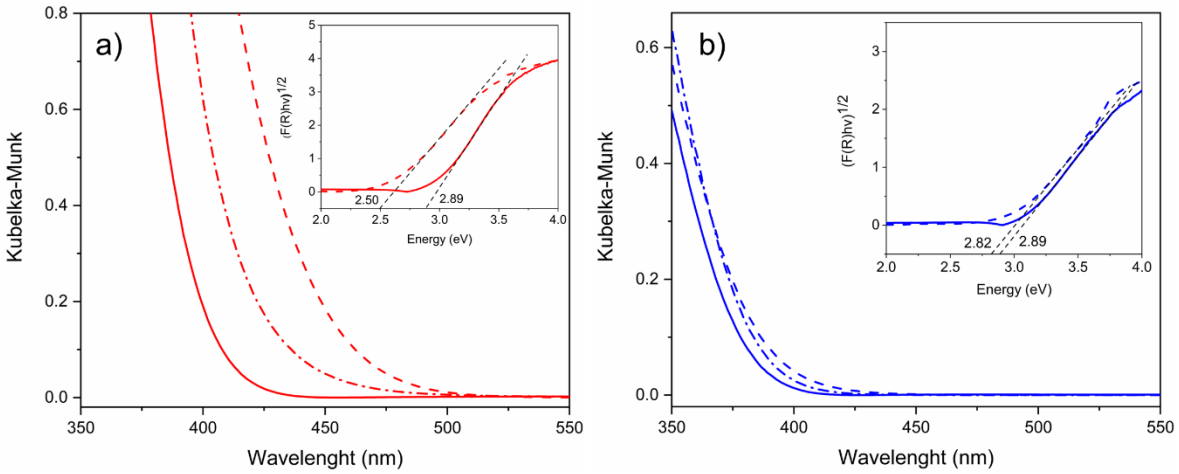

Figure S8. DRS UV-Vis spectra of the a) UiO-66($Ce_{0.5}Zr_{0.5}$) and b) UiO-66($Ce_{0.05}Zr_{0.95}$). Tauc plots are reported in the insets. As-synthesized (solid line), activated at 110ºC (dash line) and re-exposed to the atmosphere (dash dot line) UiO-66 materials

FT-IR CO adsorption

When Zr was introduced on the final UiO-66 material in an equimolar proportion ($Ce_{0.5}Zr_{0.5}$), new bands at 3674, 3668 and 3660 cm^{-1} can be observed in the IR spectrum after the activation process (see Figure S7a). The band at 3674 cm^{-1} is assigned with the ν(OH) stretching mode of (μ_3-OH)Zr_6.[5] The blue shift observed in the M-OH band when Zr is exchanged by Ce suggests stronger O-H bonds in the case of Zr_6 node due to its higher electronegativity.[6] The other bands at 3668 and 3660 cm^{-1} have been ascribed in the literature with (μ_3-OH)$CeZr_5$ nodes and (μ_3-OH)Ce_2Zr species in Ce_xZr_{6-x} clusters with x>1, respectively.[7] Moreover, the peak at 3651 cm^{-1} is consequence to the (μ_3-OH)Ce_6 cluster. Finally, in the IR spectrum of the UiO-66($Ce_{0.05}Zr_{0.95}$) sample activated at 110ºC, two different OH contributions were observed. These two at 3676 and 3670 cm^{-1} are assigned to (μ_3-OH)Zr_6 and (μ_3-OH)$CeZr_5$ clusters (see Figure S7b).[7] When CO was introduced in the cell at Liquid Nitrogen Temperature (LNT), the ν(OH) stretching bands are red-shifted in all the cases (see Figure S7, left panels). However, in the case of UiO-66($Ce_{0.5}Zr_{0.5}$), two different contributions were observed since the different (μ_3-OH)Zr_6 and (μ_3-OH)Ce_6 cluster nature (see Figure S7a, left panel). IR peaks at 2153 and 2136 cm^{-1} are observed in all the cases, which have been associated with CO interacting with OH groups and physisorbed, respectively (see Figure S7, right panels). Moreover, a band at 2127 cm^{-1} was too observed and it is often ascribed to the CO-Ce^{3+} interaction (see Figure S7, right panels).

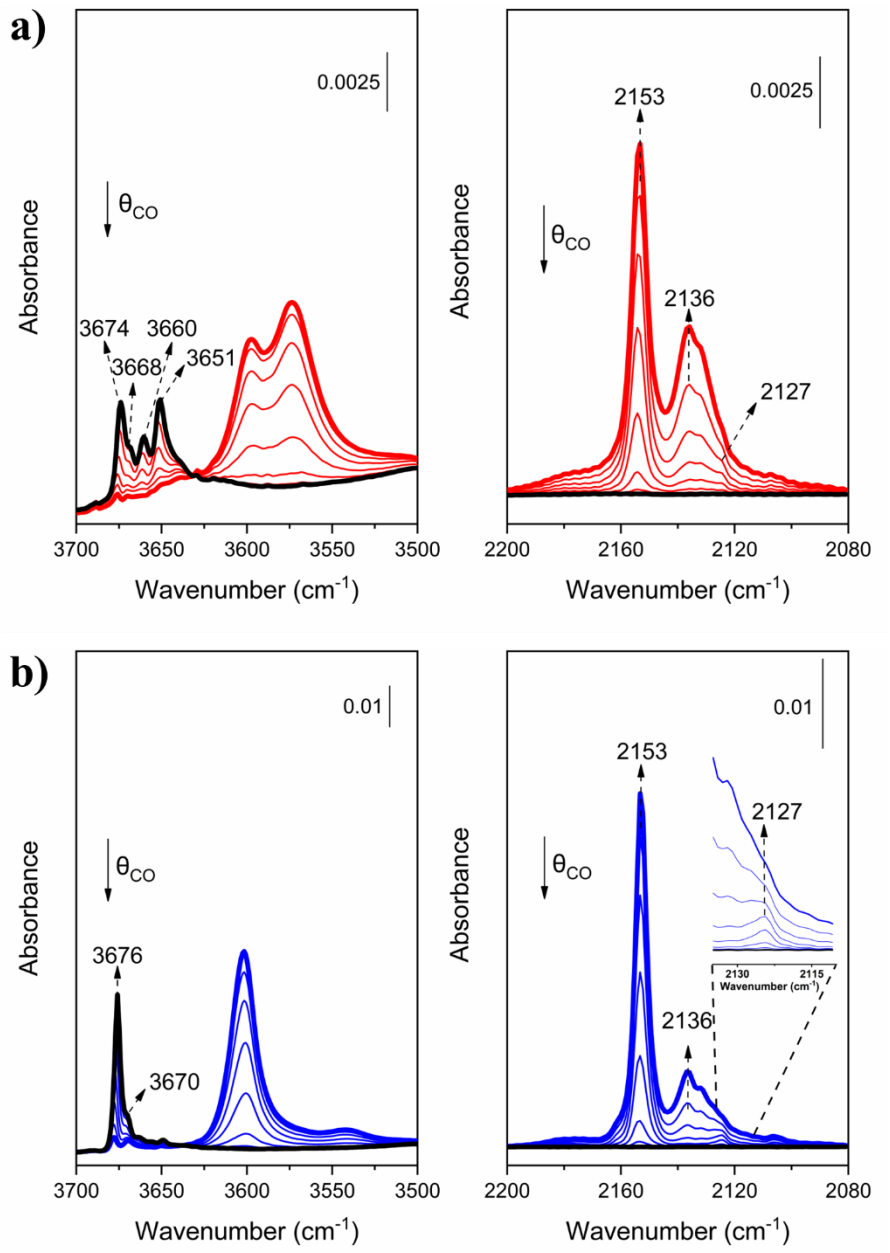

Figure S9. FT-IR spectra collected during CO desorption at LNT on a) UiO-66($Ce_{0.5}Zr_{0.5}$) and b) UiO-66($Ce_{0.05}Zr_{0.95}$).

For comparison purposes, the normalized FT-IR spectra in respect to the sample thickness collected at CO coverage of ~2 mbar for the Ce-based materials were plotted in Figure S8. The main difference between them is the absorbance of the band related with the interaction of OH groups and CO (2153 cm^{-1}). The highest absorption in this band was observed for the UiO-66($Ce_{0.05}Zr_{0.95}$) material at the same CO coverage. This fact means that the OH amount is larger in this sample than in the other two.

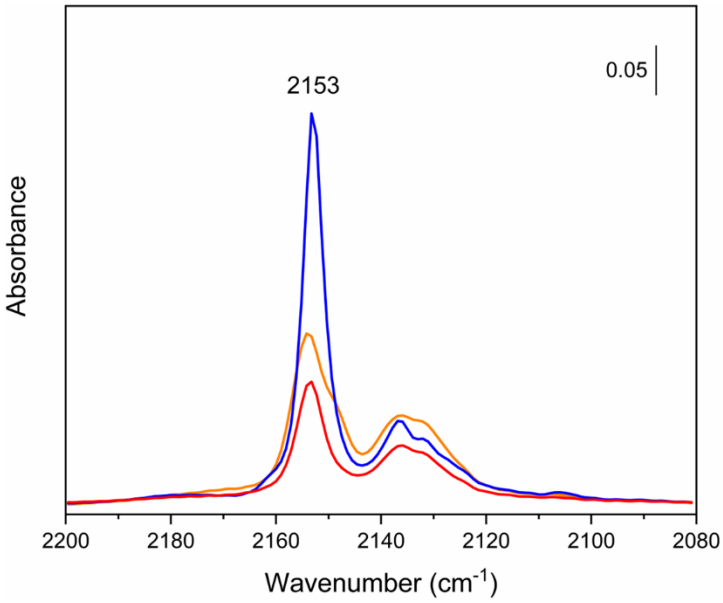

Figure S10. Comparison between FT-IR spectra collected at ~2 mbar CO coverage for UiO-66(Ce) (orange line), UiO-66($Ce_{0.5}Zr_{0.5}$) (red line) and UiO-66($Ce_{0.05}Zr_{0.95}$) (blue line).

REFERENCES

[1] R. Shannon, Revised effective ionic radii and systematic studies of interatomic distances in halides and chalcogenides, Acta Crystallogr. Sect. A. 32 (1976) 751–767. https://doi.org/10.1107/S0567739476001551.

[2] M. Ronda-Lloret, I. Pellicer-Carreño, A. Grau-Atienza, R. Boada, S. Diaz-Moreno, J. Narciso-Romero, J.C. Serrano-Ruiz, A. Sepúlveda-Escribano, E. V Ramos-Fernandez, Mixed-Valence Ce/Zr Metal-Organic Frameworks: Controlling the Oxidation State of Cerium in One-Pot Synthesis Approach, Adv. Funct. Mater. 31 (2021) 2102582. https://doi.org/https://doi.org/10.1002/adfm.202102582.

[3] M. Lammert, C. Glißmann, N. Stock, Tuning the stability of bimetallic Ce(iv)/Zr(iv)-based MOFs with UiO-66 and MOF-808 structures, Dalt. Trans. 46 (2017) 2425–2429. https://doi.org/10.1039/c7dt00259a.

[4] T. Tsoncheva, R. Ivanova, J. Henych, M. Dimitrov, M. Kormunda, D. Kovacheva, N. Scotti, V.D. Santo, V. Štengl, Effect of preparation procedure on the formation of nanostructured ceria-zirconia mixed oxide catalysts for ethyl acetate oxidation: Homogeneous precipitation with urea vs template-assisted hydrothermal synthesis, Appl. Catal. A Gen. 502 (2015) 418–432. https://doi.org/10.1016/j.apcata.2015.05.034.

[5] L. Valenzano, B. Civalleri, S. Chavan, S. Bordiga, M.H. Nilsen, S. Jakobsen, K.P. Lillerud, C. Lamberti, Disclosing the complex structure of UiO-66 metal organic framework: A synergic combination of experiment and theory, Chem. Mater. 23 (2011) 1700–1718. https://doi.org/10.1021/cm1022882.

[6] T. Islamoglu, A. Atilgan, S.Y. Moon, G.W. Peterson, J.B. Decoste, M. Hall, J.T. Hupp, O.K. Farha, Cerium(IV) vs Zirconium(IV) Based Metal-Organic Frameworks for Detoxification of a Nerve Agent, Chem. Mater. 29 (2017) 2672–2675. https://doi.org/10.1021/acs.chemmater.6b04835.

[7] C. Atzori, K.A. Lomachenko, J. Jacobsen, N. Stock, A. Damin, F. Bonino, S. Bordiga, Bimetallic hexanuclear clusters in Ce/Zr-UiO-66 MOFs: In situFTIR spectroscopy and modelling insights, Dalt. Trans. 49 (2020) 5794–5797. https://doi.org/10.1039/d0dt01023e.